

Article

Capacity Assessment of Existing RC Columns

Francesca Vecchi and Beatrice Belletti *

Department of Engineering and Architecture, University of Parma, Parco Area delle Scienze 181/A,
43124 Parma, Italy; francesca.vecchi@unipr.it

* Correspondence: beatrice.belletti@unipr.it

Abstract: Existing reinforced concrete (RC) members, designed in accordance with obsolete codes, are often characterized by high stirrup spacing. The collapse mechanisms generated by high stirrup spacing are typically related to the buckling of longitudinal reinforcement and can be accentuated when corrosion takes place. In this paper, new refined material constitutive laws for steel, including inelastic buckling and corrosion of reinforcement, are implemented in a fixed crack model suitable for RC elements subjected to cyclic loadings called the PARC_CL 2.1 crack model. The effectiveness of the proposed model is validated through comparison with available experimental data and analytical predictions. Finally, the proposed model is used to calibrate correction coefficients to be applied to current codes formulation for the ultimate rotational capacity prediction of non-conforming elements subjected to buckling phenomena and characterized by corrosion of reinforcing bars.

Keywords: buckling; existing RC elements; energy dissipation; nonlinear finite element analysis



Citation: Vecchi, F.; Belletti, B. Capacity Assessment of Existing RC Columns. *Buildings* **2021**, *11*, 161. <https://doi.org/10.3390/buildings11040161>

Academic Editors: Rita Bento

Received: 28 February 2021

Accepted: 12 April 2021

Published: 14 April 2021

Publisher's Note: MDPI stays neutral with regard to jurisdictional claims in published maps and institutional affiliations.



Copyright: © 2021 by the authors. Licensee MDPI, Basel, Switzerland. This article is an open access article distributed under the terms and conditions of the Creative Commons Attribution (CC BY) license (<https://creativecommons.org/licenses/by/4.0/>).

1. Introduction

It is estimated that 60% of the existing buildings in Italy were built in areas classified as non-seismic at the time of construction [1]. A large part of these buildings date back to the post-war period, so they were typically designed and built before seismic codes came into force. Consequently, they are characterized by lack of details, poor material characteristics, and/or corrosion of reinforcements.

The low percentage of transverse reinforcement and poor bond conditions determine that dissipative regions, such as column ends, can exhibit brittle failure mechanisms. Indeed, during loading inversions, the buckling of bars is avoided until the concrete cover avoids the development of high compressive deformations in the steel bars. On the contrary, when the concrete cover crushes, the compressive steel strains increase with the buckling of the bars, determining the collapse of the member [2,3]. This type of failure mode involves, in particular, columns of old buildings that are generally characterized by insufficient transverse reinforcement (high stirrup spacing) and a sub-dimensioned cross-section. For this reason, in existing reinforced concrete (RC) frame structures, the prediction of the column deformation capacity is crucial for structural ductility assessment [4].

As suggested by current Codes [5], the seismic capacity of existing RC structures can be evaluated by means of non-linear finite element analysis (NLFEA). However, such methods of analysis require knowledge of the real post-elastic rotational capacities of the structural element by defining yielding, peak resistance, and acceptable resistance decay. In addition, in the case of non-linear cyclic analysis of strength and stiffness, degradation models, as well as hysteretic rules, have to be defined. All these parameters can significantly influence the assessment of the ultimate rotational capacity, generally evaluated referring to a fixed resistance decay (usually assumed to be equal to 20%) with respect to the peak resistance. This definition is strongly dependent on the complex phenomena influencing the post-elastic deformation behavior, above all when structural elements are affected by buckling phenomena or have suffered from corrosion processes. In particular, the energy dissipation capacity of corroded RC structures might be overestimated when the buckling of reinforcing bars is neglected, especially in the case of corrosion.

In this framework, the likelihood of achieving a reliable prediction of the structural behavior using NLFEA depends on the definition of an accurate theoretical model characterized by realistic constitutive laws of materials and steel-to-concrete interaction.

In the literature, many authors have proposed constitutive laws for steel, including buckling [6–17]. These formulations have recently been extended for corroded elements and implemented in the NLFE program, specifically by adopting fiber models for beam finite elements [18]. However, even if, in engineering practice, fiber models are widely used, they can only consider flexural non-linearity but not non-linearity induced by shear or torsion. Nevertheless, when the columns of existing buildings are subjected to lateral displacements caused by earthquakes, they may experience formation of critical inclined cracks followed by buckling of longitudinal rebars. Structural modelling by adopting solid elements, such as membrane, shell, or brick finite elements, allows us to predict the shear failure mode or the combined flexural—shear failure mode.

The purpose of the present paper is the definition of a reliable numerical model able to assess the seismic capacity of non-conforming buildings and develop effective strengthening techniques. For this reason, a modelling approach based on multi-layered shell element modelling is presented in this paper. The non-linear response of multi-layered shell elements is evaluated using a new version of the PARC_CL 2.1 crack model (where PARC_CL 2.1 stands for Physical Approach for Reinforced Concrete under Cyclic Loading) [19]. The PARC_CL 2.1 crack model is a user subroutine developed for Abaqus [20] code that incorporates constitutive laws for steel that are able to take into account the buckling of longitudinal rebars. It is the author's opinion that this aspect represents a relevant novelty in the available literature. In particular, two different constitutive laws for steel, which have shown good performance in representing local buckling, have been implemented: the Monti and Nuti model [6] and the Kashani et al. model [15]. The proposed model has been successfully applied to the analysis of RC structures subjected to monotonic, cyclic, and dynamic loading [21,22]. In addition, based on literature results and existing empirical equations, formulations for corroded elements are also included [23,24].

For the first attempt, the proposed model is validated through comparison with experimental tests carried out at the University of Bergamo on one corroded and one uncorroded RC column that failed due to buckling of longitudinal reinforcement [25]. To this end, the experimental cyclic load-drift curve, the dissipated energy, and the ultimate chord rotation are compared with those obtained from NLFEA. Once validated, the proposed PARC_CL 2.1 crack model is used to carry out a parametric analysis on RC columns by varying the longitudinal reinforcement diameter and the stirrup spacing, and also includes the corrosion of reinforcements.

In addition, the applicability of the formulation proposed in Eurocode 8-part 3 [5] for the estimation of the ultimate chord rotation of non-conforming elements is evaluated for corroded reinforcements. Because this formulation is not able to take into account the severity of buckling and, most of all, the corrosion of reinforcement, a reductive coefficient is proposed as a function of the mass loss of the longitudinal reinforcement.

Finally, some comparisons between analytical and NLFEA results are provided in terms of resistance and ductility of un-corroded and corroded columns to highlight the cases where the formulations provided by the codes for existing members require further adjustment to allow reliable and safe structural verifications.

2. Materials and Methods

2.1. The PARC_CL 2.1 Crack Model for RC Elements

The PARC_CL 2.1 crack model is based on a total strain fixed crack approach and assumes reinforcement smeared in the hosting concrete element. More information about the model is available in Belletti et al. [19]. The new release incorporates formulations for corroded RC elements as well as constitutive laws for steel able to take into account the buckling of reinforcing bars. In particular, three constitutive laws for the simulation of the cyclic behavior of steel are implemented: the Menegotto and Pinto [26] model, the Monti

and Nuti model [6] (successively modified [27]), and the Kashani et al. model [15]. The latter two models have been recently implemented with the aim of extending the feasibility of the PARC_CL 2.1 crack model to the analysis of existing RC members with high stirrup spacing, in which the buckling of longitudinal reinforcement is expected. In this regard, one of the main parameters governing the buckling phenomena is the slenderness ratio, λ , i.e., the ratio between the stirrup spacing and the longitudinal bar diameter.

The Monti and Nuti [6] model incorporates a set of hardening rules, generated by the plastic deformation of the bars after the achievement of the yield stress, into the widely used stress-strain relationship of Menegotto and Pinto [26]. In particular, the Monti and Nuti model [6] is characterized by a kinematic and an isotropic component, differently from the Menegotto and Pinto formulation [26], which considers only the strain isotropic hardening. The authors observed that the buckling occurs when λ exceeds a critical value, λ_{cr} , equal to 5. Indeed, only when λ exceeds the critical value is the monotonic response affected by the buckling effect. In this latter case, after the reaching of the yield stress in compression, the absolute value of the compressive stress decreases with decreasing deformations; Figure 1a.

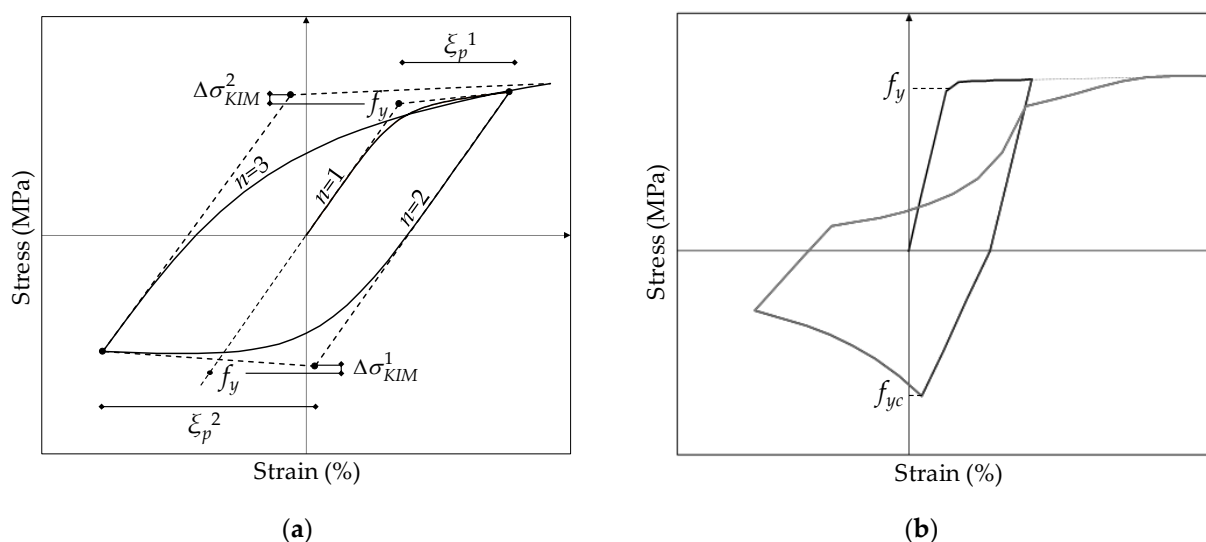


Figure 1. Constitutive law for steel including buckling: (a) Monti and Nuti model and (b) Kashani et al. model.

The yield stress, both in tension and in compression, referred to the $n+1$ half-cycle, σ_0^{n+1} , is defined in Equation (1):

$$\sigma_0^{n+1} = f_y \cdot \text{sign}(-\zeta_p^n) + \Delta\sigma_{KIM}^{n+1} \quad (1)$$

where f_y is the initial value of the yield strength, ζ_p^n is the plastic excursion, and $\Delta\sigma_{KIM}^{n+1}$ is the additional contribution due to the kinematic and isotropic hardening, defined as in Equation (2):

$$\Delta\sigma_{KIM}^{n+1} = P\Delta\sigma_{KM}^n + (1 - P)\Delta\sigma_I^n \cdot \text{sign}(-\zeta_p^n) \quad (2)$$

P is the weight attributed to each rule (isotropic $\Delta\sigma_I^n$, kinematic and memory $\Delta\sigma_{KM}^n$). Its value ranges between 0 and 1 and can be calibrated based on the experimental results [6]. The kinematic rule is coupled with the memory rule to account for the capacity of the material to memorize the plastic path followed.

The Monti and Nuti model [6] therefore presents the advantage of a simple and continuous function for the definition of the stress; however, it was calibrated according to the results obtained for a limited set of reinforcements. In particular, the parameters of the model are calibrated for steel rebar Feb44 with a yield stress equal to 450 MPa, with slenderness ratio until 11. However, existing RC structures characterized by inadequate

stirrup spacing could reach a value of slenderness ratio higher than 11. This is the most important limitation of the model.

Starting from the observation of bare bars with a yield strength between 400 and 500 MPa and $8 \leq \lambda \leq 30$, Kashani et al. [15] proposed a new stress-strain model for steel that was able to take into account the buckling of longitudinal rebar and low-cycle high amplitude fatigue; Figure 1b. According to experimental [28] and parametric [29] studies, the Kashani et al. model [15] considers that reinforcements do not buckle for $\lambda < 6$. In this case, the compressive behavior can be assumed to be equal to the tensile one. For $6 < \lambda < 8$, the sample buckles but the post-yield softening in compression is not influenced, and for this reason it can be assumed as elastic perfectly plastic. Instead, when $\lambda \geq 8$, a compressive softening curve is observed.

In Figure 2 is shown a comparison between the experimental response of a bare bar subjected to buckling phenomena [29] and the numerical results obtained using different steel models. The yielding strength of the bare bar was equal to 540 MPa with a slenderness ratio equal to 10. In general, it can be observed that the Menegotto and Pinto model is able to estimate, with good approximation, the tensile stress values but, due to its formulation, it is not able to simulate the softening behavior in compression caused by buckling. Indeed, the stress-strain response is symmetric in tension and compression without showing cyclic degradation. Instead, the Monti and Nuti [6] and the Kashani et al. [15] models are able to approximate both the tensile and compressive stress. On the other hand, when large strain values are reached, the Monti and Nuti model [6] tends to overestimate the results, both in reloading from compression to tension and in the compression branch. Instead, the Kashani et al. [15] model is able to simulate both the tensile and compressive response in terms of achieved stress.

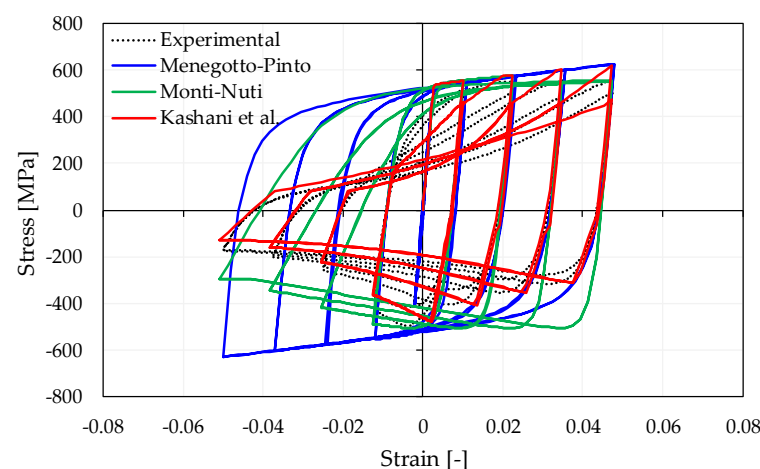


Figure 2. Comparison between non-linear finite element (NLFE) analyses obtained using the PARC_CL 2.1 crack model and experimental results.

2.2. The PARC_CL 2.1 Crack Model for RC Corroded Elements

It is not uncommon that existing buildings suffer corrosion of reinforcement. Corrosion can cause premature concrete crushing, size reduction of reinforcements, degradation of mechanical properties of steel and concrete, and degradation/breaking of the stirrups, with consequence on the seismic response and the failure mode of the RC elements. For this reason, new formulations for damaged concrete and corroded reinforcements have been introduced in the PARC_CL 2.1 crack model to simulate the behavior of corroded structural elements.

2.2.1. Reinforcing Bars

The most common approach to corrosion is the reduction of the cross-sectional area of the corroded reinforcements. However, this simplified approach does not take ductility reduction into account. For this reason, a variation of the stress-strain relationship of the

corroded reinforcement is proposed in Kashani et al. [15] and implemented in the PARC_CL 2.1 crack model. The proposed formulations account for a reduction of mechanical properties due to pitting corrosion, decreasing both the capacity and the ductility developed by reinforcements. In particular, the yield strength and the ultimate strain in tension of a corroded bar can be evaluated according to Equations (3) and (4), respectively; Figure 3a.

$$f'_y = f_y(1 - \beta_s \cdot \psi) \quad (3)$$

$$\epsilon'_u = \epsilon_u(1 - \beta_e \cdot \psi) \quad (4)$$

where f_y and f'_y are the yield strength of the un-corroded and the corroded bar, respectively; ϵ_u and ϵ'_u are the ultimate strain of the un-corroded and the corroded bar, respectively; ψ is the mass loss percentage; β_s is a coefficient equal to 0.005; and β_e is set equal to 0.05 for bars in concrete.

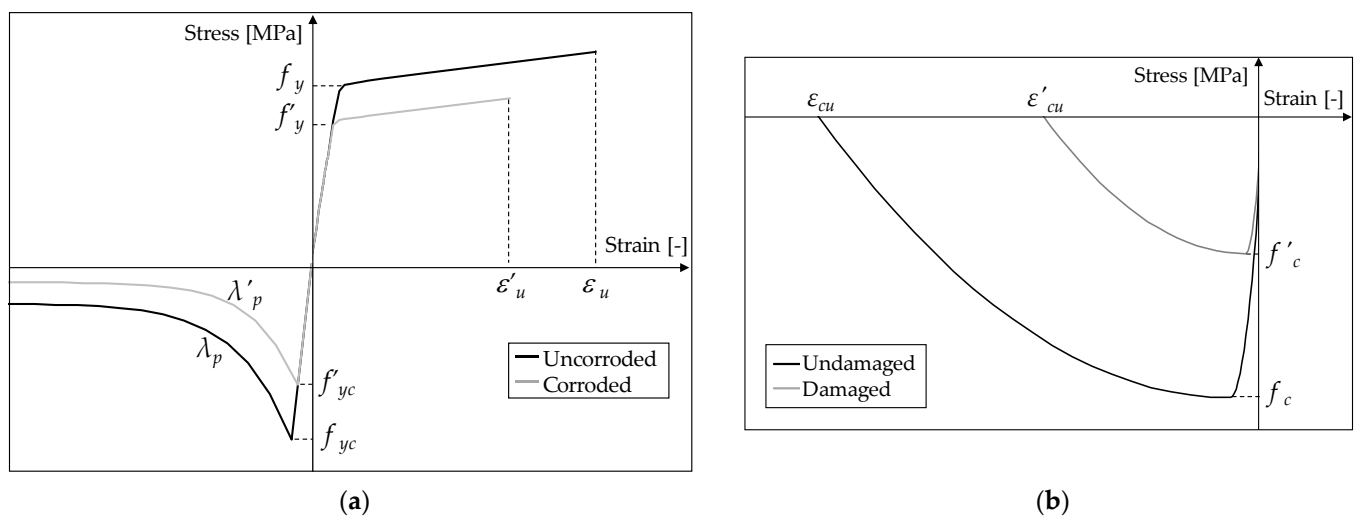


Figure 3. Constitutive relationship in case of corrosion: (a) reinforcing bars and (b) concrete.

It is worth mentioning that the Kashani et al. [15] model also considers the effect of corrosion on the cross section, considering an average reduced cross section diameter (effective section), ϕ' ; Equation (5).

$$\phi' = \phi \sqrt{1 - \psi} \quad (5)$$

Finally, the compression response of reinforcing bars is modified according to Equation (6):

$$f'_{yc} = f_y(1 - \beta \cdot \psi) \quad (6)$$

where f'_{yc} is the buckling strength of the corroded bar deduced by the mean sectional area of the corroded bar (as a function of the mass loss) and f_y is the yield strength of the un-corroded bar; Figure 3a. β represents the influence of non-uniform pitting corrosion, and its value is a function of the slenderness ratio, as reported in Prota et al. [14].

2.2.2. Concrete Elements

The greater volume of corroded steel can cause delamination and spalling of the concrete cover, and consequently the strength of the concrete in compression can be compromised. In this regard, Coronelli and Gambarova [30] provided a simple formulation to reduce the compressive strength of the damaged concrete; Equation (7):

$$f'_c = \frac{f_c}{1 + K \cdot \epsilon_1 / \epsilon_{c0}} \quad (7)$$

where f_c is the compressive strength of undamaged concrete; f'_c is the compressive strength of damaged concrete; K is a coefficient related to the bar roughness and diameter; ε_{c0} is the strain at the peak compressive strength, f_c ; and ε_1 is the average strain in the cracked concrete, which can be obtained from Equation (8):

$$\varepsilon_1 = \frac{\pi n \phi (v_{rs} - 1) (1 - 0.1 \sqrt{100 - \psi})}{b_0} \quad (8)$$

where n is the number of bars in compression; v_{rs} is the ratio of volumetric expansion of the oxides with respect to the un-corroded material, which can be taken to be equal to 2 [31]; and b_0 is the section width in the un-corroded state.

Finally, Figure 3b shows the compressive behavior of damaged and undamaged concrete elements.

3. Results

3.1. Validation of the PARC_CL 2.1 Crack Model

To validate the proposed PARC_CL 2.1 crack model, a set of two experimental RC columns, cyclically tested by Meda et al. [25], have been selected. The columns were 1.80 m in height with a square 300 mm × 300 mm section and were reinforced with 4Ø16 longitudinal steel bars. They were characterized by poor material characteristics, Table 1, and large stirrup spacing (Ø8@300 mm at the column base). In particular, one column was subjected to artificial corrosion of the longitudinal reinforcement until there was a mass loss of about 20%, while stirrups were protected from corrosion. An axial load of 400 kN was applied and, finally, a cyclic horizontal displacement history was imposed at a height of 1.5 m from the column foundation connection.

Table 1. Mechanical properties of columns adopted in NLFEA.

	Concrete				Longitudinal Reinforcement			
	f_c [MPa]	f_{ct} [MPa]	E_c [MPa]	λ	f_y [MPa]	f_{yc} [MPa]	f_u [MPa]	E_s [MPa]
Un-corroded	19.0	1.5	25,000	19	520.0	−520.0	620.0	210,000
Corroded	9.40	1.5	25,000	21	468.0	−391.0	500.6	210,000

The numerical model is shown in Figure 4. For evaluating the proper and stable mesh size, a mesh sensitivity analysis has been performed [32]. The columns have been modelled using four-node shell elements (S4, [20]) with full integration and three Simpson integration points for each layer along the thickness. The element thickness has been subdivided into seven layers to properly describe the reinforcement layout. An elastic material has been adopted for the foundation, while different materials have been used for the columns to distinguish the slenderness ratios of longitudinal rebars and reinforcement ratios of stirrups.

With reference to the x-y-z system of Figure 4, the displacements at the base in the z direction, the displacements of the extreme nodes of the foundation in the x direction, and the displacements of all the nodes of the column in the y direction have been prevented.

More details of the mechanical properties adopted in NLFEA for the selected columns are provided in Table 1. For the corroded column, because the stirrups were protected in the experimental test, they have been modelled with reference to the mechanical properties of un-corroded rebars. The concrete cover elements have been modelled using damaged properties, as shown in Table 1, while the concrete core elements have been assumed to be undamaged. Finally, the corroded properties of the longitudinal reinforcement have been evaluated in accordance with the formulations presented in Section 2.2.

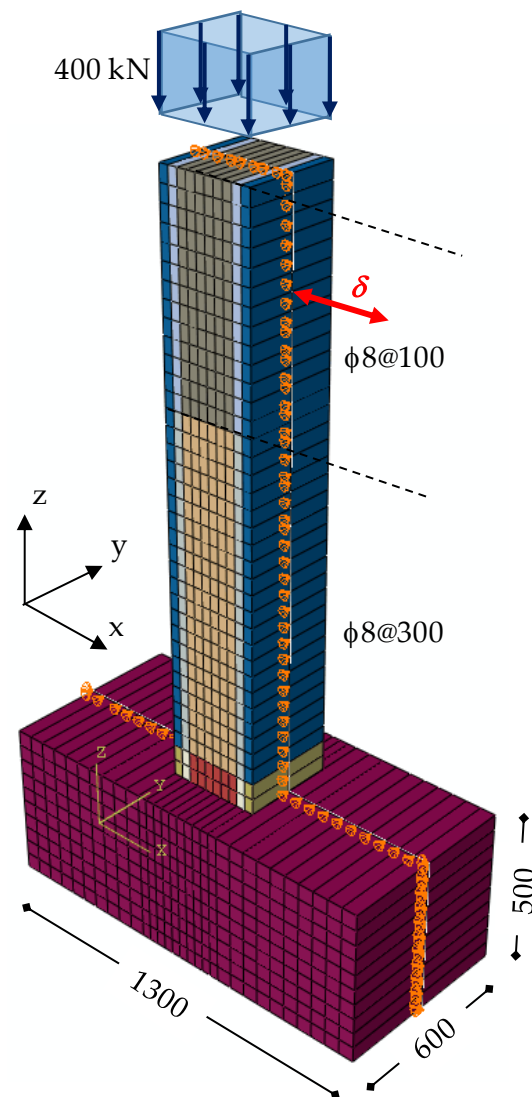


Figure 4. Geometry of the numerical model [mm].

The NLFEA has been performed using displacement control method. A regular type Newton–Raphson incremental iterative method has been applied.

Because the spacing between stirrups was inadequate, both the columns developed the instability of the longitudinal reinforcement at the column base. In order to highlight the differences between considering and disregarding the buckling phenomena in the prediction of the nonlinear behavior of RC elements, the nonlinear analysis have been performed using the three constitutive laws for steel implemented in the PARC_CL 2.1 model: the Menegotto and Pinto model, the Monti and Nuti model, and the Kashani et al. model. In this regard, the actual slenderness ratio has been adopted for the numerical analysis conducted using the Kashani et al. model for steel, while the maximum acceptable value of slenderness (equal to 11) has been used for the Monti and Nuti analysis. On the contrary, since the Menegotto and Pinto model is not dependent on the slenderness ratio's values of the longitudinal bars, the buckling phenomena has been neglected.

Figure 5 shows the comparison between the load-drift curves obtained by NLFE analysis, carried out with the PARC_CL 2.1 crack model, and the experimental one, both for the corroded and the un-corroded column.

Observing Figure 5a, until a drift equal to 2% (corresponding to the beginning of the softening behavior), the results of the NLFE analyses are similar because the concrete controls the behavior of the column and the steel does not exhibit buckling. Instead, for

drifts larger than 2%, the concrete starts to crush in compression and consequently the longitudinal reinforcements start to work in compression. Starting from this point, the experimental curve shows a softening behavior, while the NLFE analysis conducted with the Menegotto and Pinto model keeps on growing. Similarly, the Monti and Nuti model does not catch the peak load and overestimates the ultimate capacity. Furthermore, the stiffness in the unloading and reloading branches is also overestimated, highlighting the inability of an accurate simulation of the hysteretic cycles. On the contrary, the Kashani et al. model exhibits a more pronounced softening behavior, closer to the experimental one in respect of the Monti and Nuti one. Furthermore, the Kashani et al. model permits us to predict with better accuracy the hysteretic behavior of the cycles, both for low and high levels of drift. Certainly, the fitting of results obtained using the Monti and Nuti model is affected by the difference between the actual slenderness of the longitudinal reinforcing bars with respect to the intrinsic limit of the model. For other case studies characterized by slenderness ratio lower or equal to 11, the Monti and Nuti model can provide good response prediction, as can the Kashani et al. model. In that case, the Monti and Nuti model could be easier to implement and could provide a more stable convergence thanks to the simplicity of its formulation.

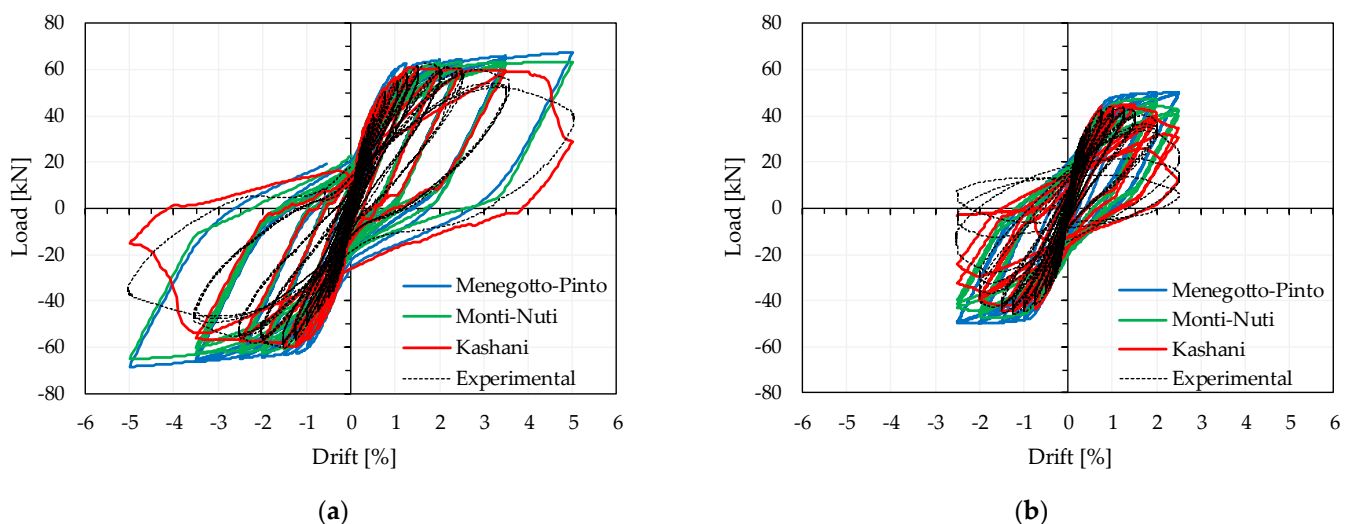


Figure 5. Comparison between the experimental and numerical responses in terms of load-drift curve: (a) un-corroded column, (b) corroded column.

Figure 5b shows the results obtained for the corroded column, where the same trend of the un-corroded column is observed. Indeed, once again, the Kashani et al. model returns the most realistic result in terms of maximum peak load and stiffness during the unloading-reloading cycles.

Observing Figure 5, it is possible to conclude that any steel model not including buckling is unable to capture the actual ultimate resistance of an RC member characterized by high stirrup spacing.

It is commonly recognized that, in predictive numerical simulations, the estimation of dissipated work is a matter of interest and its prevision is highly dependent on realistic modelling of possible structural damages under cyclic loadings. In this regard, Figure 6 shows the normalized cumulative work, i.e., the cumulative work of each half cycle divided by the total cumulative work of the experimental column. The cumulative energy dissipation is defined as the sum of the energy dissipated in each cycle, while the half cycle number corresponds to the change of the drift sign.

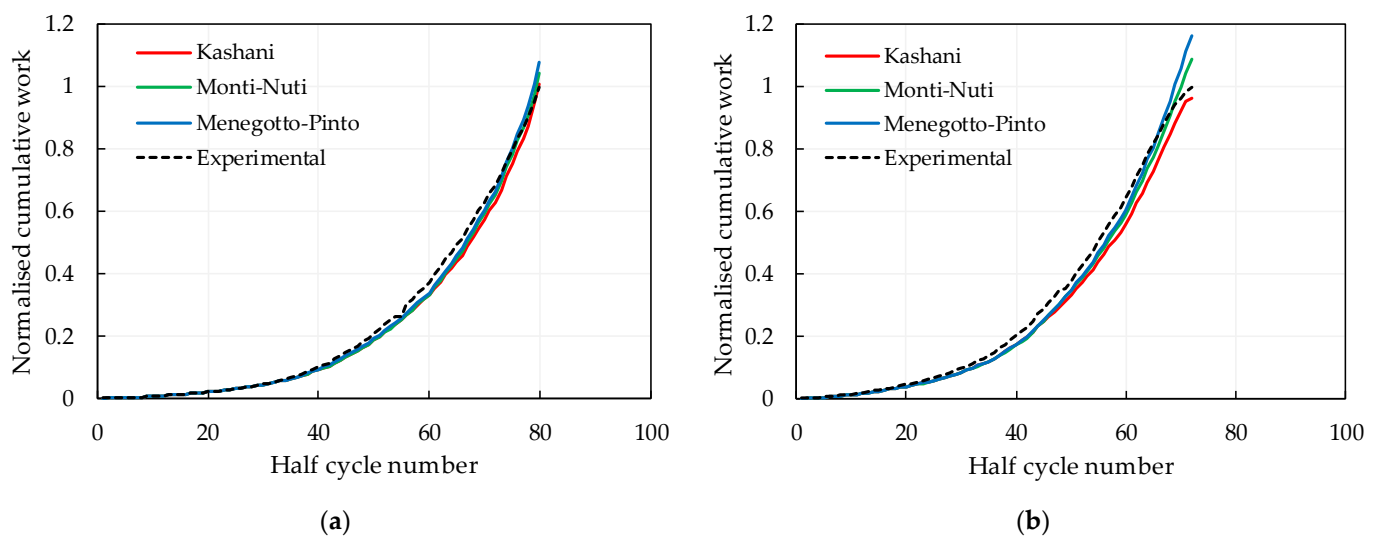


Figure 6. Comparison between the experimental and numerical responses in terms of energy dissipation capacity: (a) un-corroded column, (b) corroded column.

Figure 6b demonstrates that disregarding the inelastic buckling of reinforcing bars can lead to significant overestimation of the energy dissipation capacity of deteriorated RC structures. However, it is worth noting that this criterion is not sufficient to highlight the potentiality of adopting steel models that include buckling. Indeed, all the NLFEA results obtained for the un-corroded column are similar and are in good agreement with the experimental one, Figure 6a. This is due to the fact that both the load-drift curves obtained using the Menegotto and Pinto model and the Monti and Nuti model overestimate the load and at the same time underestimate the stiffness during the unloading-reloading cycle.

3.2. Parametric Analysis on Buckling Effects in Existing Un-Corroded Columns

Once validated, the numerical model has been extended to further case studies with the aim of studying the influence of the longitudinal reinforcement diameter, ϕ , the stirrup spacing, s , and corrosion of longitudinal reinforcement on the cyclic behavior of the columns.

Starting from the reference un-corroded column tested by Meda et al. [25], columns with longitudinal bar diameters equal to 14 mm, 16 mm (reference), 18 mm, 20 mm, 22 mm, and 24 mm have been studied, keeping the other properties unchanged. In addition, the cases in which the stirrup spacing is 100 mm, 150 mm, 200 mm, 300 mm (reference), and 400 mm have been analyzed. Finally, the reference column has been analyzed considering mass losses for longitudinal reinforcement equal to 10%, 20% (reference), and 30, with and without corrosion of the stirrups. The study of the corroded columns has also been extended to the cases with a longitudinal reinforcement diameter equal to 20 and 24 mm.

The columns have been modelled by adopting the same modelling strategies presented in the previous paragraph and by using the three constitutive laws for steel available in the PARC_CL 2.1 crack model. Furthermore, the NLFEA have been carried out up to failure, in order to highlight the potentiality of adopting models able to consider the buckling phenomenon of longitudinal rebars, when necessary.

A critical evaluation of the ability of the proposed models to catch the ductility of an existing RC column can be made through the evaluation of the ultimate chord rotation capacity. Generally, the rotational capacity, θ_u , corresponds to a 20% strength decay on the envelope curve. The envelope curve includes extreme points of imposed displacement cycles and in-cycle softening branches, if present, as shown in Figure 7.

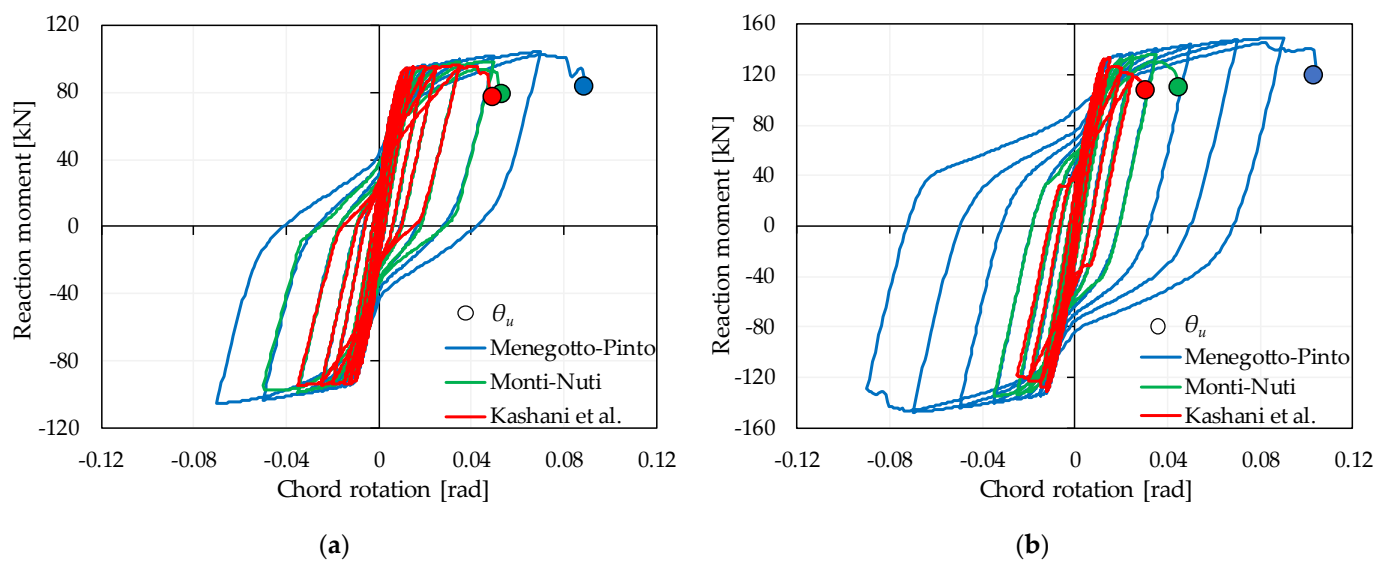


Figure 7. Reaction moment-chord rotation curve obtained from NLFEA: (a) column s150, (b) column $\phi 22$.

For the sake of brevity, only two examples will be reported in order to explain the adopted procedure. The first analyzed case study refers to the column with stirrup spacing equal to 150 mm (column s150); Figure 7a. The second case study refers to the column characterized by longitudinal reinforcement equal to $4\phi 22$ (column $\phi 22$); Figure 7b. As shown in Figure 7, the ultimate chord rotation obtained by using the Menegotto and Pinto model is much higher than those obtained by using the Kashani et al. model. This is due to the fact that the strain field developed by the Kashani et al. model, as well as the Monti and Nuti model, reaches the buckling of the longitudinal reinforcement and the crushing of the concrete cover, resulting in a more pronounced softening behavior.

Figure 8 summarizes the ultimate chord rotation values obtained for all the analyzed case studies. As expected, the ultimate chord rotation of the un-corroded reference column (longitudinal bars diameter equal to $\phi 16$ and stirrup spacing equal to 300 mm) is predicted with high accuracy using the Kashani et al. model. The variation of the longitudinal reinforcement diameter, as well as the stirrup spacing, causes a variation of the slenderness ratio, up to values equal to 25. With the increase of the slenderness ratio, the differences between the ultimate chord rotation prediction obtained using the Kashani et al. model and the Monti and Nuti model increases while, for a slenderness ratio less than 11, the chord rotations are comparable.

Figure 8 also reports the ultimate chord rotation obtained using the formulation proposed for an existing building in EN 1008-3:2005 [5] in Section A.3.2.2 (Limit state of near collapse); Equation (9):

$$\theta_u = \frac{1}{\gamma_{el}} 0.016 \cdot (0.3^v) \cdot \left[\frac{\max(0.01; \omega')}{\max(0.01; \omega)} f_c \right]^{0.225} \left(\frac{L_v}{h} \right)^{0.35} 25^{(\alpha \rho_{sx} \frac{f_{yw}}{f_c})} (1.25^{100 \rho_d}) \quad (9)$$

where γ_{el} is equal to 1.5 for primary seismic elements and to 1 for secondary seismic elements; h is the depth of cross-section; L_v is the ratio moment/shear at the end section; $v = N/(A_c f_c)$, where N is the axial load and A_c is the concrete gross area; ω , ω' is the mechanical reinforcement ratio of the tension (including the web reinforcement) and compression, respectively, longitudinal reinforcement; f_c and f_{yw} are the concrete compressive strength (MPa) and the stirrup yield strength (MPa), respectively, directly obtained as mean values from in-situ tests and from the additional sources of information, appropriately divided by the confidence factors; ρ_{sx} is the ratio of transverse steel parallel to the direction x of loading; ρ_d is the steel ratio of diagonal reinforcement (if any) in each diagonal direction; and α is the confinement effectiveness factor.

The values of chord rotation calculated according to Equation (9) apply to elements with ribbed bars, seismically detailed and without the lapping of longitudinal bars in the vicinity of the end region, where yielding is expected (plastic hinge region). The correction coefficient applied to members with ribbed bars without seismic detailing is equal to 0.825. This latter constant coefficient does not take into account the severity of the buckling phenomena, which may degrade the cyclic response of columns, as demonstrated in Figure 8.

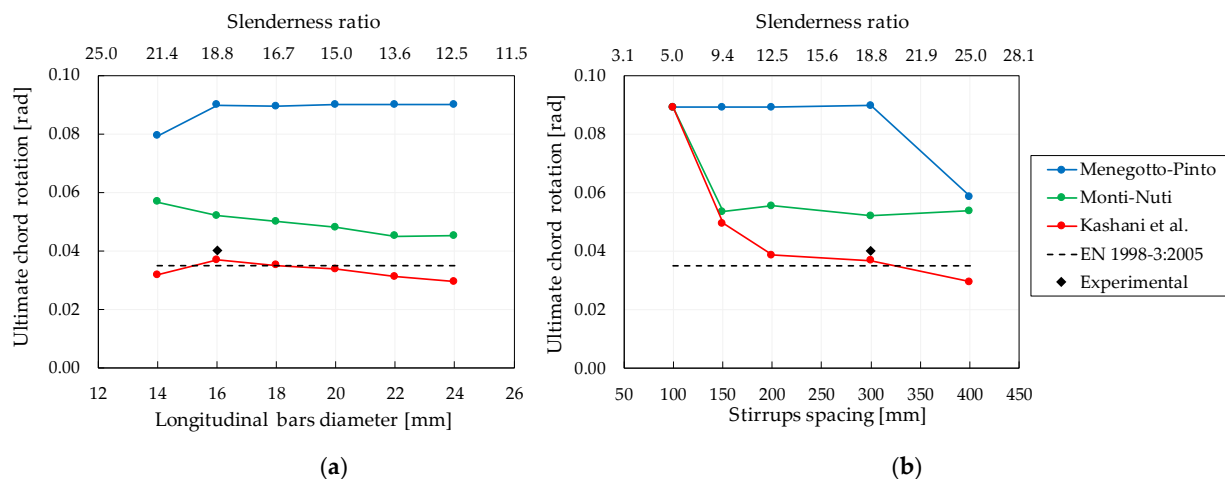


Figure 8. Comparison of ultimate chord rotation for different values of: (a) longitudinal bars diameter, ϕ , (b) stirrups spacing, s .

Figure 8 shows that neglecting the buckling of rebars in NLFEA can cause an overestimation of the ultimate chord rotation. Comparing the analytical value of the chord rotation with the experimental result of the un-corroded column, it emerges that Equation (9) is on the safe side. Indeed, Equation (9) was calibrated on the basis of a large database of representative specimens and extended to poorly detailed members, so it also implicitly considers the case of existing members that exhibited buckling of longitudinal rebars [33]. On the other hand, Equation (9) is not affected by the variation of the longitudinal reinforcement diameter because, in the examined case studies, the reinforcement in compression and tension are symmetric, meaning that symmetric sections with different amounts of longitudinal reinforcement have the same ductility. It is also independent of the stirrup spacing because, in Equation (9), the ratio of transverse steel is multiplied by the confinement effectiveness factor, α , which, for stirrups with inadequate anchorage (usually with 135-degree hook along the length of the member), can be assumed to be equal to 0.

The prediction of the ultimate chord rotation evaluated by NLFEA by adopting the Menegotto–Pinto model or the Monti–Nuti model give the results of being unsafe because the capacity, in terms of ductility, is higher than the capacity obtained by considering the buckling of longitudinal reinforcement.

Figure 8b shows that, in the case of columns with a low value of stirrup spacing ($s100$), where buckling phenomena are not affecting the column cyclic response, the ultimate chord rotation evaluated with the Menegotto–Pinto, Monti–Nuti, and Kashani et al. models result the same. Furthermore, Figure 8b shows that, in the case of columns with a low value of stirrup spacing ($s100$, $s150$), Equation (9) provides a too conservative estimation of the ultimate rotation capacity.

Figure 8b shows that, in the case of high stirrup spacing ($s200$, $s300$, $s400$), the parametric analysis on un-corroded RC columns highlights the need to adopt more refined constitutive laws in order to obtain more realistic predictions. Indeed, for high stirrup spacing ($s300$, $s400$) Equation (9) could display an unsafe result that is lower than the ductility capacity evaluated by considering buckling phenomena.

3.3. Parametric Analysis on Buckling Effects in Existing Corroded Columns

The parametric study has been extended to the analysis of corroded RC columns. In particular, the reference column (longitudinal reinforcement equal to $\varphi 16$) has been analyzed considering different scenarios of mass loss; Figure 9a. Because it is demonstrated that the Monti–Nuti model is not able to return a reliable result for a high value of slenderness ratio, the parametric analysis has been conducted using the Menegotto and Pinto model and the Kashani et al. one. As expected, the Kashani et al. model is able to provide more realistic results in respect of the Menegotto and Pinto model, which widely overestimates the chord rotation at failure.

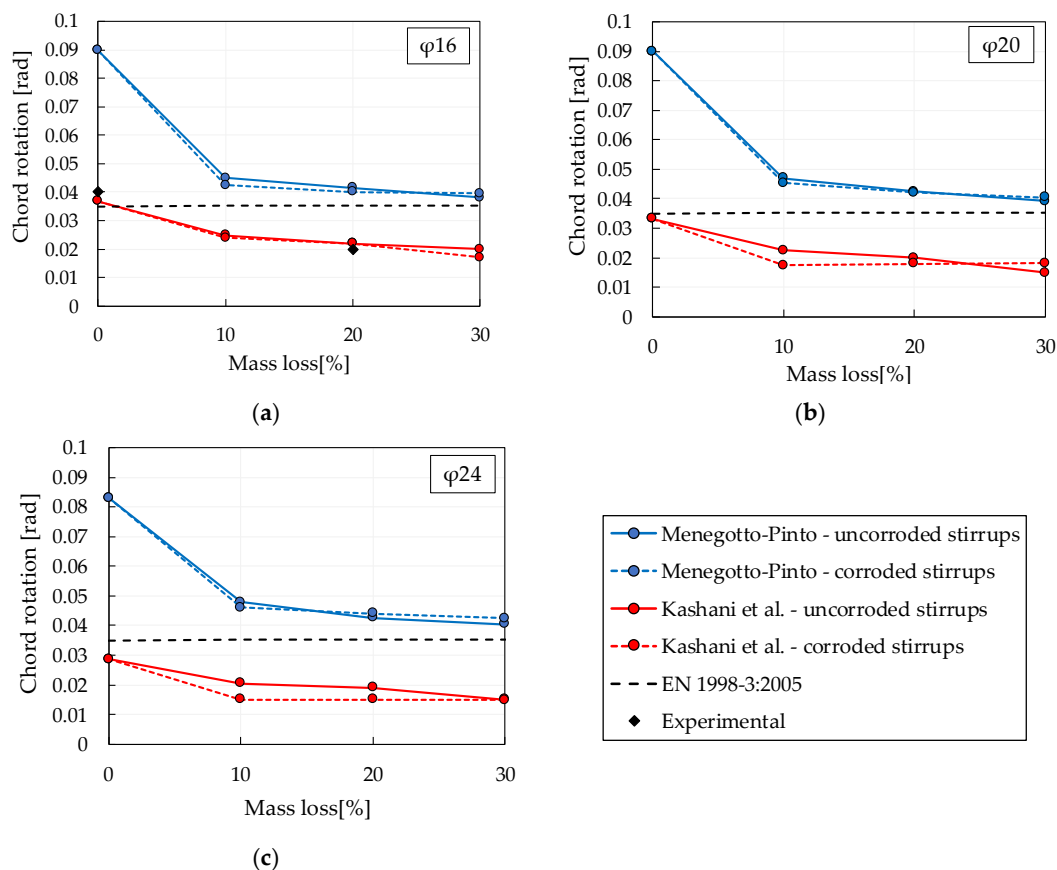


Figure 9. Comparison of ultimate chord rotation in the function of the mass loss for different values of longitudinal reinforcement diameter: (a) $\varphi 16$, (b) $\varphi 20$, and (c) $\varphi 24$.

In addition, the study is extended to longitudinal reinforcement diameters equal to 20 and 24 mm, also considering the corrosion of stirrups; Figure 9. Indeed, stirrups are typically corroded in real structures and are generally exposed to higher aggression of corrosion than longitudinal reinforcement, compromising the shear capacity and causing a reduction of the compressive capacity and ductility of RC columns.

In the case of corroded stirrups, the NLFEM have been carried out by assuming the corrosion of stirrups equal to 3.5 times the corrosion of longitudinal reinforcements, according to experimental evidences [34]. In particular, for the case study with a mass loss of the longitudinal reinforcement equal to 30%, stirrups have not been considered. The yield strength and the ultimate tensile strain have been modified according to Equations (3) and (4), respectively. In addition, the influence of stirrup corrosion on the behavior of longitudinal reinforcement has been taken into account by assuming the buckling length as twice the case of un-corroded stirrups.

Because the stirrup spacing for the analyzed case studies is high (equal to 300 mm), the corrosion of stirrups does not significantly affect the ultimate chord rotation. However, the

ultimate strain of corroded stirrups has been reduced, and for this reason stirrup rupture has been observed in NLFEA for mass loss higher than 20% [23].

The predicted ultimate chord rotations obtained from NLFEA are compared with Equation (9). As shown in Figure 9, the ultimate chord rotation provided by NLFEA is in good agreement with the results obtained using Equation (9) for un-corroded columns (mass loss equal to 0%), while it diminishes with the increase of the mass loss differently to Equation (9). It is worth mentioning that Equation (9) does not provide any suggestion for corroded elements and for this reason a constant value for all the considered corrosion levels is obtained. This constant value overestimates the ductility of the reference corroded RC column by about 75%.

Finally, the ultimate chord rotations obtained using the Kashani et al. model is compared with Equation (9) for columns with longitudinal reinforcement equal to 16 mm, 20 mm, and 24 mm, subjected to different corrosion levels (0%, 10%, 20%, and 30%); Figure 10a. The ultimate chord rotation provided by NLFEA diminishes with the increase of the mass loss and the longitudinal reinforcement parameter, while Equation (9) is not affected by these parameters. This explains the large scatter between the numerical and analytical chord rotation obtained for high values of mass loss.

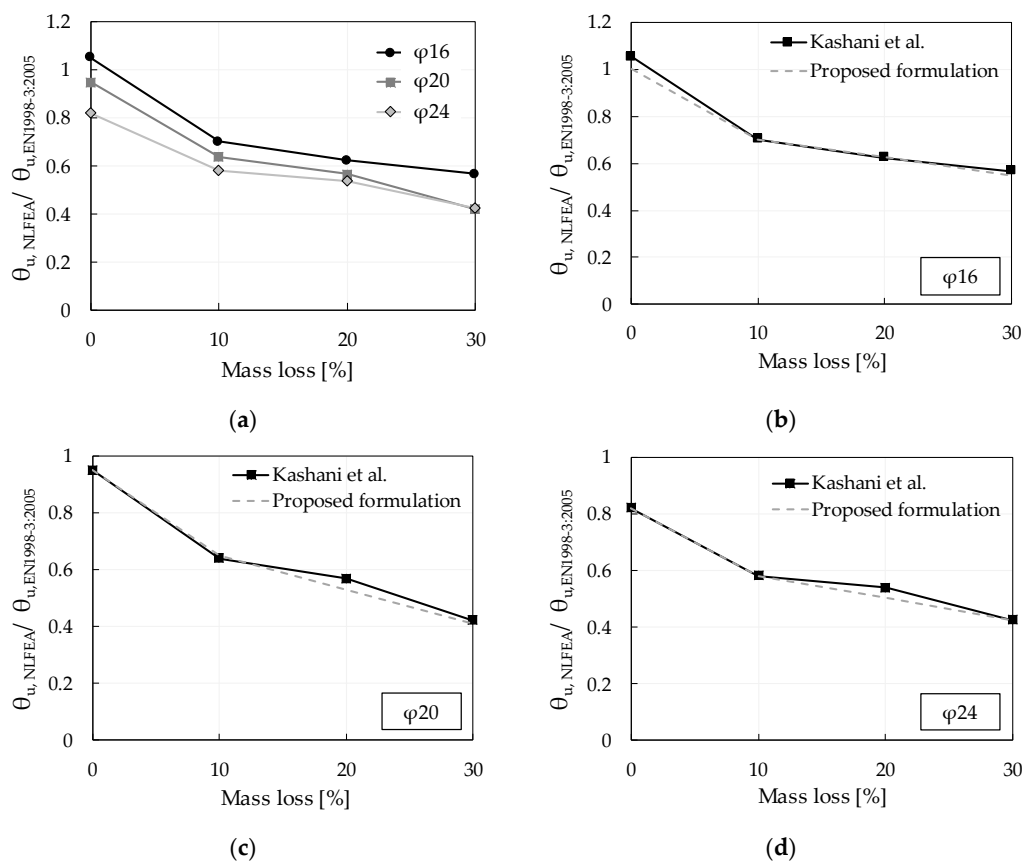


Figure 10. Normalized chord rotation in the function of the mass loss: (a) for different longitudinal reinforcement diameters. Proposed formulation for: (b) $\phi 16$, (c) $\phi 20$, and (d) $\phi 24$.

With the aim of extending Equation (9) to the study of existing corroded RC elements, a reductive coefficient value, α_{COR} , to be multiplied by Equation (9), is proposed. For this reason, in Figure 10 the ratio between the ultimate chord rotation obtained from NLFEA (adopting the Kashani et al. model) and those obtained from Equation (9) is plotted in the function of the mass loss. As shown, the reductive coefficient, α_{COR} , varies with the corrosion level and with the tendency of longitudinal bars to buckle.

On the basis of the obtained results, the following bi-linear expression is proposed:

$$\alpha_{COR} = \begin{cases} a - b \cdot \psi & \text{if } 0 < \psi \leq \psi_{lim} \\ \psi_{lim} \cdot a - c \cdot (\psi - \psi_{lim}) & \text{if } \psi_{lim} < \psi \end{cases} \quad (10)$$

where ψ_{lim} is equal to 10%, while a , b , c , are parameters reported in Table 2 for the analyzed case studies.

Table 2. Parameter values for the proposed formulation.

	$\phi 16$	$\phi 20$	$\phi 24$
a	1	0.95	0.82
b	0.03	0.03	0.023904
c	0.0075	0.012	0.007806

3.4. Comparison between Analytical and NLFEA Capacity Prediction

The capacity prediction, both in terms of resistance and ductility obtained by analytical and NLFEA are compared in this section. Furthermore, the ductile or brittle failure mode exhibited by the analyzed columns is evaluated. This is of particular interest because, in existing buildings, the possible onset of a brittle failure of the RC column represents the crisis of the whole structure.

According to CNR-DT 212/2013 [35], ductile and the brittle behavior can be evaluated by adopting analytical methods at the intersection of the resistance versus chord rotation relationships that describe the flexural and the shear non-linear response; Figure 11. The shear failure in the elastic field (Case A) is achieved when this intersection occurs before flexural-yielding, determining a brittle failure. The shear failure in the plastic field (Case B) is achieved when the intersection occurs after flexural yielding. Finally, ductile failure (Case C) is achieved when the ultimate chord rotation is reached before the intersection.

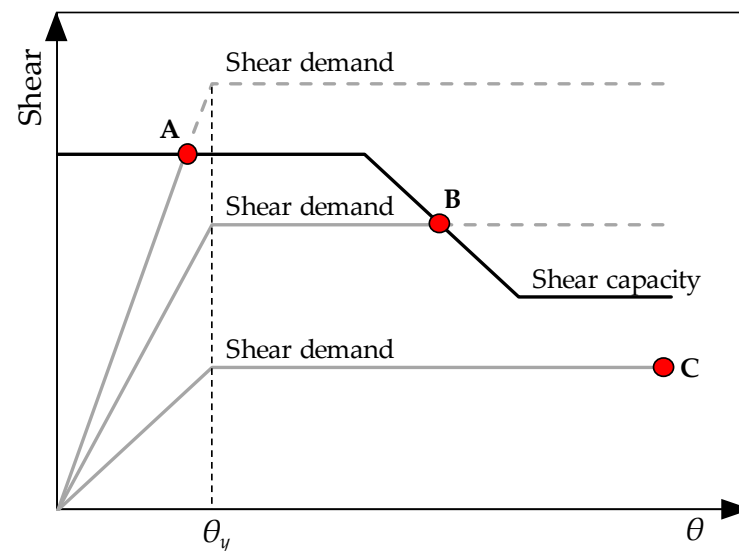


Figure 11. Shear-bending interaction and failure modes.

The flexural capacity of a corroded column can be evaluated from the equilibrium conditions of internal forces in the cross section, considering the corroded properties of reinforcements. Furthermore, because it has been observed that the concrete cover of longitudinal bars spalled off due to corrosion, a reduced cross section is considered.

According to Biskinis et al. [36], the nominal shear strength is calculated as the sum of the contribution of concrete, V_C , the contribution of transversal reinforcement, V_W , and of the axial load, V_N . The concrete contribution can be evaluated as:

$$V_C = \left[1 - 0.05 \min \left(5; \mu_{\Delta}^{pl} \right) \right] \cdot \left\{ 0.16 \max(0.5; 100 \rho_{tot}) \cdot \left[1 - 0.16 \min \left(5; \frac{L_V}{h} \right) \right] \cdot \sqrt{f_c} \cdot A_c \right\} \quad (11)$$

The contribution of transversal reinforcement is given by:

$$V_W = \left[1 - 0.05 \min \left(5; \mu_{\Delta}^{pl} \right) \right] \cdot \rho_w \cdot b_w \cdot z \cdot f_{yw} \quad (12)$$

and the axial load contribution is given by:

$$V_N = \frac{h-x}{2 \cdot L_V} \min(N; 0.55 A_c \cdot f_c) \quad (13)$$

where h is the depth of the cross-section, x is the compression zone depth, ρ_{tot} is the total longitudinal reinforcement ratio, ρ_w is the transverse reinforcement ratio, and z is the length of the internal lever arm.

The plastic part of the displacement ductility factor can be estimated following Equation (14):

$$\mu_{\Delta}^{pl} = \frac{\theta_u - \theta_y}{\theta_y} \quad (14)$$

where θ_u and θ_y are the ultimate chord rotation and the yielding rotation, respectively. θ_y is the chord rotation at yield, as defined by Equation (15) for RC columns:

$$\theta_y = \Phi_y \frac{L_v}{3} + 0.0013 \cdot \left(1 + 1.5 \frac{h}{L_v} \right) + 0.13 \cdot \Phi_y \cdot \frac{d_{bL} \cdot f_y}{\sqrt{f_c}} \quad (15)$$

Table 3 reports the comparison between the failure mode obtained by analytical calculation and by NLFEA. As expected, the analytical predictions are on the safe side, providing lower capacities than the NLFEA ones.

In the case of corroded stirrups or in the case of un-corroded columns with $\phi 24$ longitudinal rebar, brittle failure modes are expected by adopting analytical methods. On the contrary, flexural failures are detected by NLFEA, except for column $\phi 16$ with mass loss equal to 20 and 30% in the case of the corrosion of stirrups. In those cases, the NLFEA exhibited a shear failure with the rupture of the stirrups at the column base. This aspect confirms that too conservative shear resistance formulations can lead to failure modes' predictions not respecting the actual column behavior. Therefore, in future studies a new model recently provided by Biskinis and Fardis [37] will be adopted for a more accurate analytical prediction of the shear capacity of columns subjected to cyclic degradation.

According to the definition of the ductility factor provided in Equation (14), the comparison between the numerical and analytical prevision are reported in Table 3. As expected, because the ductility factor depends on the ultimate chord rotation capacity experienced by the structural element, the ductility factor obtained from NLFEA diminishes with the increase of the mass loss. Finally, Figure 12 reports the ductility factors obtained from NLFEA and analytical calculations. Once again, the results demonstrate that disregarding buckling in RC elements with high stirrup spacing causes an incorrect evaluation of the available ductility.

Table 3. Comparison between failure modes and ductility factor obtained from analytical calculations and NLFEA.

		Manual Calculation				NLFEA			
		Corrosion Level [%]	Failure Mode	V [kN]	μ_{Δ}^{pl}	Failure Mode	V_{max} [kN]	V_u [kN]	μ_{Δ}^{pl}
$\varphi 16$	Un-corroded stirrups	0	F	60.21	1.36	F	62.90	50.32	1.94
		10	F	46.94	1.26	F	54.09	43.27	1.48
		20	F	42.89	1.44	F	45.54	36.43	1.50
		30	F	39.12	1.62	F	40.89	32.71	1.27
	Corroded stirrups	10	S-F	46.94	1.26	F	52.52	42.02	1.50
		20	S	35.39	1.44	Stirrups rupture	42.48	33.99	1.44
30		S	28.08	1.62	Stirrups rupture	38.43	30.74	1.18	
$\varphi 20$	Un-corroded stirrups	0	F	78.03	1.22	F	78.65	62.92	1.92
		10	F	61.39	1.10	F	67.79	54.23	1.14
		20	F	55.11	1.27	F	56.13	44.90	1.00
		30	F	49.26	1.47	F	49.15	39.32	0.53
	Corroded stirrups	10	S	52.34	1.10	F	64.34	51.47	0.81
		20	S	40.12	1.27	F	49.85	39.88	0.94
30		S	32.28	1.47	F	45.03	36.03	1.02	
$\varphi 24$	Un-corroded stirrups	0	S	87.96	1.03	F	99.72	79.78	0.96
		10	S	72.86	0.95	F	84.63	67.70	0.55
		20	S-F	70.26	1.13	F	68.81	55.05	0.52
		30	F	61.65	1.32	F	58.88	47.11	0.50
	Corroded stirrups	10	S	58.66	0.95	F	78.85	63.08	0.50
		20	S	45.86	1.13	F	59.31	47.45	0.50
30		S	37.37	1.32	F	51.26	41.01	0.49	

F = flexural failure, S-F = shear-flexural failure, S = pure shear failure, V_{max} is the maximum load reached by NLFEA, and V_u is the load corresponding to failure.

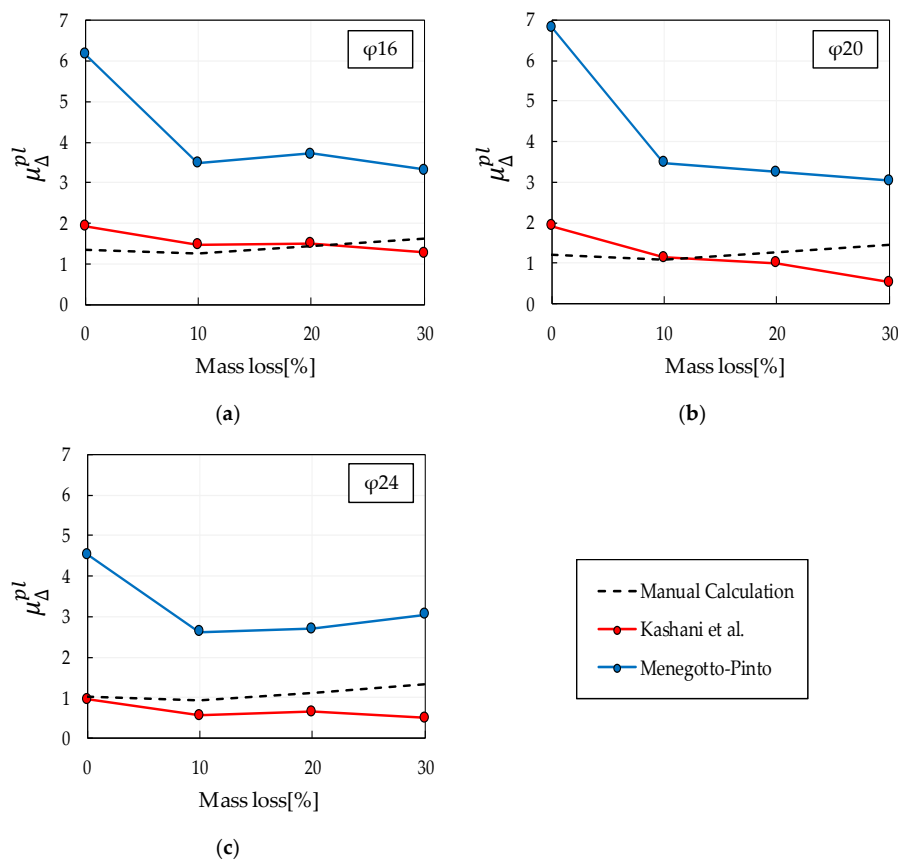


Figure 12. Ductility factors obtained from analytical calculation and NLFEA for different corrosion levels: (a) column $\varphi 16$, (b) column $\varphi 20$, and (c) column $\varphi 24$.

4. Conclusions

The most diffused reinforcing steel material models, frequently adopted in the design practice, can simulate the non-linear behavior of RC columns before the buckling failure but not the degradation effects caused by severe buckling of vertical reinforcement [38], overestimating the capacity in terms of strength and ductility. However, the buckling of longitudinal reinforcement substantially influences the response of RC existing structural elements. For this reason, a numerical crack model able to take into account the buckling failure is developed and applied to RC columns. The proposed crack model is also able to consider the corrosion effects on RC elements subjected to cyclic loadings. Based on the obtained results, the following remarks can be drawn:

- Efficient models able to take into account more realistic behavior of the materials as well as the failure mode are needed. Models for steel that include buckling avoid overestimation of the strength, energy dissipation, and ultimate capacity of the existing structure, most of all when corrosion of reinforcement occurs. Indeed, when the Menegotto and Pinto model is adopted, an overestimation of the ultimate resistance of about 10% for the un-corroded column and of about 18% for the corroded column is obtained, while an ultimate chord rotation twice the value of the experimental one is found.
- Steel models that neglect the buckling of rebars are not able to capture the reduction of the resistance and ductility.
- Multi-layered shell elements could be a powerful tool for providing a more refined moment-curvature or rotation relationship that can be applied to simplified modelling techniques as lumped plasticity models or modelling with beam elements (more suitable in the case of large structures with many degrees of freedom).
- The global behavior of existing RC elements subjected to cyclic loading could also be affected by material degradation. Corrosion of reinforcement is one of the main causes of deterioration of RC structures that can anticipate the buckling phenomena, drastically reducing the ductility of the structural element.
- Current Codes do not provide indications for the assessment of corroded RC structures, causing an overestimation of the ultimate chord rotation prediction. In this framework, once validated, numerical analysis could be useful to calibrate analytical formulation provided by codes.

Author Contributions: Conceptualization, B.B. and F.V.; methodology, B.B.; software, F.V.; validation, F.V.; formal analysis, B.B.; investigation, F.V.; resources, B.B.; data curation, F.V.; writing—original draft preparation, F.V. writing—review and editing, B.B.; supervision, B.B.; project administration, B.B.; funding acquisition, B.B. All authors have read and agreed to the published version of the manuscript.

Funding: This research received no external funding.

Institutional Review Board Statement: Not applicable.

Informed Consent Statement: Not applicable.

Data Availability Statement: Not applicable.

Acknowledgments: The paper is part of the research project RELUIS 2019-2021—WP11 UR8 “Contributi normativi relativi a costruzioni esistenti in cemento armato”. The activity was carried out by the members of the University of Parma (Principal Investigator B. Belletti).

Conflicts of Interest: The authors declare no conflict of interest.

References

1. Parisi, M.A.; Maggio, E.; Marini, C.; Sumini, V. Edifici storici in calcestruzzo armato in zona sismica: Valutazione delle risorse. In Proceedings of the XV Convegno ANIDIS L'Ingegneria Sismica in Italia, Padova, Italy, 30 June–4 July 2013.
2. Wallace, J.W.; Massone, L.M.; Bonelli, P.; Dragovich, J.; Lagos, R.; Lüders, C.; Moehle, J. Damage and implications for seismic design of RC structural wall buildings. *Earthq. Spectra* **2012**, *28*, 281–299. [[CrossRef](#)]

3. Massone, L.M. Fundamental principles of the reinforced concrete design code changes in Chile following the Mw 8.8 earthquake in 2010. *Eng. Struct.* **2013**, *56*, 1335–1345. [[CrossRef](#)]
4. Cosenza, E.; Manfredi, G.; Verderame, G.M. Seismic assessment of gravity load designed R.C. frames: Critical issues in structural modelling. *J. Earthq. Eng.* **2002**, *6*, 101–122. [[CrossRef](#)]
5. *Eurocode 8: Design Provisions for Earthquake Resistance of Structures—Part 3: Assessment and Retrofitting of Buildings*; CEN European Standard EN1998-3; European Committee for Standardisation: Brussels, Belgium, 2005.
6. Monti, G.; Nuti, C. Nonlinear cyclic behaviour of reinforcing bars including buckling. *J. Struct. Eng.* **1992**, *118*, 3268–3284. [[CrossRef](#)]
7. Dodd, L.L.; Restrepo-Posada, J.I. Model for predicting cyclic behaviour of reinforcing steel. *J. Struct. Eng.* **1995**, *121*, 433–445. [[CrossRef](#)]
8. Gomes, A.; Appleton, J. Nonlinear cyclic stress-strain relationship of reinforcing bars including buckling. *Eng. Struct.* **1997**, *10*, 822–826. [[CrossRef](#)]
9. Pantazopoulou, S.J. Detailing for Reinforcement Stability in RC Members. *J. Struct. Eng.* **1998**, *124*, 623–632. [[CrossRef](#)]
10. Rodriguez, M.E.; Botero, J.C.; Villa, J. Cyclic stress-strain behaviour of reinforcing steel including the effect of buckling. *J. Struct. Eng.* **1999**, *125*, 605–612. [[CrossRef](#)]
11. Bayrak, O.; Sheikh, S. Plastic hinge analysis. *J. Struct. Eng.* **2001**, *127*, 1092–1100. [[CrossRef](#)]
12. Dhakal, R.P.; Maekawa, K. Path-dependent cyclic stress–strain relationship of reinforcing bar including buckling. *Eng. Struct.* **2002**, *24*, 1383–1396. [[CrossRef](#)]
13. Cosenza, E.; Prota, A. Experimental behaviour and numerical modelling of smooth steel bars under compression. *J. Earthq. Eng.* **2006**, *10*, 313–329. [[CrossRef](#)]
14. Prota, A.; de Cicco, F.; Cosenza, E. Cyclic Behaviour of Smooth Steel Reinforcing Bars: Experimental Analysis and Modeling Issues. *J. Earthq. Eng.* **2009**, *13*, 500–519. [[CrossRef](#)]
15. Kashani, M.M.; Lowes, L.N.; Crewe, A.J.; Alexander, N.A. Phenomenological hysteretic model for corroded reinforcing bars including inelastic buckling and low-cycle fatigue degradation. *Comput. Struct.* **2015**, *156*, 58–71. [[CrossRef](#)]
16. Dhakal, R.P.; Maekawa, K. Modeling for postyield buckling of reinforcement. *J. Struct. Eng.* **2002**, *128*, 1139–1147. [[CrossRef](#)]
17. Kashani, M.M.; Lowes, L.N.; Crewe, A.J.; Alexander, N.A. Finite element investigation of the influence of corrosion pattern on inelastic buckling and cyclic response of corroded reinforcing bars. *Eng. Struct.* **2014**, *75*, 113–125. [[CrossRef](#)]
18. Spacone, E.; Filippou, F.C.; Taucer, F.F. Fibre beam-column model for nonlinear analysis of RC frames: Part I—Formulation. *Earthq. Eng. Struct. Dyn.* **1996**, *25*, 711–725. [[CrossRef](#)]
19. Belletti, B.; Scolari, M.; Vecchi, F. PARC_CL 2.0 crack model for NLFEM of reinforced concrete structures under cyclic loadings. *Comput. Struct.* **2017**, *191*, 165–179. [[CrossRef](#)]
20. Abaqus 6.12. Available online: <http://www.3ds.com/> (accessed on 1 June 2016).
21. Belletti, B.; Stocchi, A.; Scolari, M.; Vecchi, F. Validation of the PARC_CL 2.0 crack model for the assessment of the nonlinear behaviour of RC structures subjected to seismic action: SMART 2013 shaking table test simulation. *Eng. Struct.* **2017**, *150*, 759–773. [[CrossRef](#)]
22. Belletti, B.; Muttoni, A.; Ravasini, S.; Vecchi, F. Parametric analysis on punching shear resistance of reinforced concrete continuous slabs. *Mag. Concr. Res.* **2018**, *71*, 1083–1096. [[CrossRef](#)]
23. Belletti, B.; Vecchi, F. A crack model for corroded reinforced concrete elements subject to cyclic loading. *Proc. Inst. Civ. Eng. Bridge Eng.* **2021**. accepted.
24. Vecchi, F.; Belletti, B. Ultimate chord rotation of corroded reinforced concrete columns subjected to cyclic loading. In Proceedings of the Fib CACRCS DAYS 2020, On-Line Event, 1–4 December 2020.
25. Meda, A.; Mostosi, S.; Rinaldi, Z.; Riva, P. Experimental evaluation of the corrosion influence on the cyclic behaviour of RC columns. *Eng. Struct.* **2014**, *76*, 112–123. [[CrossRef](#)]
26. Menegotto, M.; Pinto, P.E. Method of analysis for cyclically loaded R.C. plane frames including changes in geometry and non-elastic behaviour of elements under combined normal force and bending. In Proceedings of the Symposium on the Resistance and Ultimate Deformability of Structures Acted on by Well Defined Repeated Loads, Lisbon, Portugal, 2–5 September 1973.
27. Zhou, Z.H.; Nuti, C.; Lavorato, D. Modified Monti-Nuti Model for Different Types of Reinforcing Bars Including Inelastic Buckling. *Appl. Mech. Mater.* **2016**, *847*, 166–172. [[CrossRef](#)]
28. Nakamura, H.; Higai, T. Modeling of Nonlinear Cyclic Behaviour of Reinforcing Bars. *ACI SP* **2002**, *205*, 273–292.
29. Kashani, M.M.; Crewe, A.J.; Alexander, N.A. Nonlinear cyclic response of corrosion-damaged reinforcing bar with the effect of buckling. *Constr. Build. Mater.* **2013**, *41*, 388–400. [[CrossRef](#)]
30. Coronelli, D.; Gambarova, P. Structural Assessment of Corroded Reinforced Concrete Beams: Modeling Guidelines. *ASCE J. Struct. Eng.* **2004**, *130*, 1214–1224. [[CrossRef](#)]
31. Molina, F.J.; Alonso, C.; Andrade, C. Cover cracking as a function of rebar corrosion. II: Numerical model. *Mater. Struct.* **1993**, *26*, 532–548. [[CrossRef](#)]
32. Strauss, A.; Mandić Ivanković, A.; Benko, V.; Matos, J.; Marchand, P.; Wan-Wendner, R.; Galvão, N.; Orcesi, A.; Dobrý, J.; El Hajj Diab, M.; et al. Round-Robin Modelling of the Load-bearing Capacity of Slender Columns by Using Classical and Advanced Nonlinear Numerical and Analytical Prediction Tools. *Struct. Eng. Int.* **2021**, *31*, 118–135. [[CrossRef](#)]

33. Panagiotakos, T.B.; Fardis, M.N. Deformations of Reinforced Concrete Members at Yielding and Ultimate. *ACI Struct. J.* **2001**, *98*, 135–145.
34. Lin, H.; Zhao, Y.; Yang, J.; Feng, P.; Özbolt, J.; Ye, H. Effects of the corrosion of main bar and stirrups on the bond behavior of reinforcing steel bar. *Constr. Build. Mater.* **2019**, *225*, 13–28. [[CrossRef](#)]
35. CNR-DT 212/2013. *Istruzioni per la Valutazione Affidabilistica della Sicurezza Sismica di Edifici Esistenti*; CNR: Rome, Italy, 2013. (In Italian)
36. Biskinis, D.E.; Roupakias, G.K.; Fardis, M.N. Degradation of shear strength of reinforced concrete members with inelastic cyclic displacement. *ACI Struct. J.* **2004**, *101*, 773–783.
37. Biskinis, D.; Fardis, M.N. Cyclic shear resistance for seismic design, based on monotonic shear models in fib Model Code 2010 and in the 2018 draft of Eurocode 2. *Struct. Concr.* **2020**, *21*, 129–150. [[CrossRef](#)]
38. Kashani, M.M.; Salami, M.R.; Goda, K.; Alexander, N.A. Non-linear flexural behaviour of RC columns including bar buckling and fatigue degradation. *Mag. Concr. Res.* **2018**, 231–247. [[CrossRef](#)]